Journal of Materials Chemistry

Cite this: J. Mater. Chem., 2012, 22, 14228

www.rsc.org/materials

PAPER

Interfacial engineering of quantum dot-sensitized TiO_2 fibrous electrodes for futuristic photoanodes in photovoltaic applications†

P. Sudhagar,[a] Victoria González-Pedro,[b] Iván Mora-Seró,*[b] Francisco Fabregat-Santiago,[b] Juan Bisquert[b] and Yong Soo Kang*[a]

Received 14th March 2012, Accepted 27th April 2012
DOI: 10.1039/c2jm31599h

Herein we report generic surface treatment approaches to improve the electronic interfaces of quantum dot-sensitized TiO_2 fiber electrodes, thereby promoting their photoanode performance. Highly dense, continuous and nanostructured TiO_2 fibrous membranes, without the inclusion of a scattering layer, unlike conventional TiO_2 particulate electrodes, showed feasible photoconversion performance under the proposed interfacial engineering modification. The proposed interfacial treatment concerns fibrous membranes both before and after calcination. The chemical vapor pre-treatment on an as-deposited fibrous membrane using tetrahydrofuran (THF) reinforces the physical contact between the fibrous membrane and the transparent conducting substrate and reduces significantly the recombination rate. In the case of post-treatment by F-ion on a fibrous surface, together with the interfacial engineering approach, the ZnS surface passivation layer markedly improves the photoanode performance of the TiO_2 fibrous membrane nearly to a factor of 3.2% with a remarkable open-circuit voltage $V_{oc} = 0.69$ V and $J_{sc} = 13$ mA cm^{-2} under 1 sun illumination (100 mW cm^{-2}). This report provides an excellent platform for studying and understanding the interfacial contacts and mechanisms related to the charge transfer at CdS/CdSe QD-sensitized TiO_2 fibrous assemblies. Such implications of this interfacial treatment strategy can be successfully extended to a wide range of photoanode candidates in energy conversion systems and confirm the effectiveness of some alternative nanostructured electrodes for the development of semiconductor-sensitized solar cells.

1. Introduction

In the context of searching for pioneer energy conversion systems, quantum dot-sensitized solar cells (QDSCs) have attracted growing interest as a potential candidate for the development of next generation photovoltaic devices.[1–4] In view of tuning the absorption spectrum of semiconductor quantum dots (QDs), probing the particle size is an efficient way to harvest the entire range of the solar spectrum.[5] In addition, owing to the unique electronic band structure, QDs can overcome the Shockley–Queisser limit of energy conversion efficiency.[6] The ability of QDs to harvest hot electrons and to generate multiple carriers makes them a viable candidate for light harvesting sensitizers in solar cells.[7–9] Several semiconductor materials[10–16] have been used as light sensitizers on wide band gap mesoporous metal oxide layers (TiO_2 and ZnO) due to their low cost and simple sensitization processing.

Recently, extending the light harvesting wavelength through panchromatic metal sulfide sensitizers including PbS/CdS,[16,17] CdS/CdSe,[18,19] and QDs–dye[20–23] configurations offers new avenues to attain high conversion efficiency. Currently QDSCs display an appreciable efficiency of about 5–6%,[24,25] yet there is ample room available to drive the conversion efficiency in competition with dye-sensitized solar cells (12%).[26] In order to amplify the efficiency of QDSCs, several issues need attention, which essentially include the designing of robust and multi-functional materials for each counterpart of QDSCs (anodes, sensitizers, redox-mediators, and counter-electrodes).[27–30] Specifically, photoanode geometry[27] plays a crucial role in determining the conversion efficiency of the cells through controlling the amount of QD-loading and electrolyte penetration, but also surface recombination and light scattering. For instance, the smaller pore size (~5 to 10 nm) of particulate-shaped TiO_2 particles limits the QDs coverage on deeper layers. Such uncovered QDs on TiO_2 surfaces lead to an electron-loss pathway by means of electrolyte contact which could result in recombination and deteriorate the device performance. Furthermore, insufficient electrolyte penetration into the deeper

[a]World Class University Program Department of Energy Engineering, and Center for Next Generation Dye-Sensitized Solar Cells, Hanyang University, Seoul 133-791, South Korea. E-mail: kangys@hanyang.ac.kr
[b]Photovoltaic and Optoelectronic Devices Group, Departament de Física, Universitat Jaume I, 12071 Castelló, Spain. E-mail: sero@fca.uji.es

† Electronic supplementary information (ESI) available: XRD and XPS results of QD-sensitized TiO_2 fibers are included. See DOI: 10.1039/c2jm31599h

pores of the smaller-pore TiO_2 framework also restricts the hole-carriers scavenging at TiO_2–QD interfaces. In addition, QDs show a faster recombination rate and a more complicated electron-loss pathway than organic dyes;[31,32] therefore a wide pore size geometry of TiO_2 has to be designed for QDSCs exclusively, without sacrificing their charge transport characteristics. In view of this, it is anticipated that a highly porous 1-D fibrous membrane with a continuous crystalline framework is the desired photoanode for QDSCs to afford sufficient QD-loading and superficial electrolyte penetration.[18,33]

Utilization of the wide pore structured 1-D photoanodes (nanotubes and nanofibers) is receiving great attention in DSSCs[34–39] and QDSCs[40] that rely on high charge collection efficiency. Their architectural advantages for superficial electrolyte penetration through vertical pores yield effective interfacial contacts with TiO_2–sensitizer interfaces. In particular, fibrous electrodes prepared by an electrospinning technique showed remarkable performance in DSSCs since they have less grain boundary density, which can overcome the trapping–detrapping loss unlike conventional nanoparticulate electrodes.[41] Archana *et al.*[42] reported that a 1D fibrous film results in a high diffusion coefficient ($D_n \approx 4.6 \times 10^{-4}$ cm^2 s^{-1}), which is nearly 3 times higher than that of the particulate electrodes ($D_n \approx 1.5 \times 10^{-4}$ cm^2 s^{-1}) under identical photoexcitation density. Furthermore, they observed less charge transport resistance and transit time in the fibrous electrode over the nanoparticle electrode. The charge transport characteristics of fibrous electrodes are responsible for their use as photoanodes for achieving feasible charge collection at QDSCs compared to conventional nanoparticle electrodes. The lower grain boundary density of 1D fibrous anodes also offers beneficial advantages in attenuating the scattering loss of free electrons to the nanoparticle electrode. On the other hand, the inclusion of nanofibers in conventional nanoparticle electrodes (composite) substantially improves the light harvesting through promoting the light-scattering pattern (analogous to antenna lobes).[33,43]

Most fibrous electrodes have been fabricated using a two-step method. After fiber synthesis, substrates are coated with the synthesized fibers, but in this case poor particle interconnectivity is detected. Continuous electrospun fibers solve this problem but peel off limitations have to be overcome. Various approaches have been demonstrated for this purpose. Song *et al.* utilized a hot press method to enhance the adhesion of the nanofiber to the substrate.[44] Similarly, chemical treatment was also employed to relax the nanofiber to yield an improved adhesion of the nanofiber to the substrate.[45] Onozuka *et al.*[46] applied a dimethyl formamide (DMF) treatment to TiO_2 fibrous electrodes, where DMF induced the swelling of the polymeric substances in the composite film and reinforced the adhesion between the substrate and fibrous membranes. This DMF treatment has improved the charge collection efficiency of DSCs by about 20% compared to untreated electrodes. Our recent work[10] also showed that the DMF treatment to the electro-spun spheroidal electrodes for CdS QD-sensitized solar cells increased the efficiency from 0.85% to 1.2% through improving the electrical contact between the fibers and the Transparent Conducting Oxide (TCO) substrate. Therefore, a generic surface treatment approach is demanded for fibrous electrodes to maintain their inter-connecting morphology as well as charge transport behavior in QDSC configurations.

In the present work, we explore the surface treatment using dimethylformamide (DMF) and tetrahydrofuran (THF) vapor on TiO_2 fibrous electrodes. We found that THF vapor treatment improves device performance compared to the untreated fibrous electrode through enhancing the photovoltage, V_{oc}, and photocurrent, J_{sc}, of the QDSCs. Here, we report the dual performance of THF. Firstly, the THF vapor etches the TiO_2 fibrous surface, modifying the density of states and reinforcing the electrical contact with the TCO substrate. Secondly, THF treatment decreases dramatically the recombination rate in the prepared QDSCs. The detailed investigation on the influence of THF treatment on charge injection and charge recombination at TiO_2–QD interfaces using impedance spectroscopy (IS) is presented. In addition to THF and DMF treatments, the effects of F ion treatment on the TiO_2 fibrous surface as well as the ZnS passivation layer on TiO_2–QD interfaces are also studied and discussed, for further improvement of QDSCs performance.

2. Experimental techniques

2.1 Fabrication of the TiO_2 fibrous photoanode

A continuous TiO_2 fibrous membrane is directly deposited on a FTO substrate using the electrospinning technique. The following solution is used for spinning (all chemicals were received from Sigma Aldrich and used without further purification): 0.53 g of polyvinyl acetate (PVAc) dissolved in 4.45 g of dimethyl formamide (DMF). After completely dissolving the PVAc in DMF, 1 g of titanium(IV) propoxide and 0.5 g of acetic acid were mixed well for 30 minutes. The resultant solution for spinning is loaded into a pumping syringe and connected to a high-voltage power supply. An electrical potential of 15 kV was applied over a collection distance of 12 cm. The electrospun fibrous membranes were collected continuously on the grounded FTO substrate for 20 minutes. Subsequently the films were sintered at 450 °C for 30 minutes in air.

For investigating the influence of surface treatment on the fibrous surface, as-deposited TiO_2 fibrous membranes were treated in two different environments before the sintering process. For DMF treatment, the samples were immersed in DMF for 10 seconds and dried at room temperature. For THF treatment, the samples were kept in an anhydrous tetrahydrofuran (THF) chamber (25 ml) without direct contact with THF for 30 minutes. After surface treatment the samples were sintered at 450 °C for 30 minutes in atmospheric air.

2.2 QD-sensitization

TiO_2 fibrous electrodes were sensitized using semiconductor quantum dots as mentioned in our earlier reports.[27] Firstly, CdS QDs were directly assembled on a TiO_2 fibrous surface by the SILAR process. The Cd^{2+} cationic and S^{2-} anionic precursors were prepared with 0.5 M cadmium acetate in ethanol and 0.5 M Na_2S in methanol, respectively. A single SILAR cycle consisted of 15 minutes of dip-coating of the fibrous electrode into each of the above-mentioned chemical baths. After each bath, the fibrous electrode was completely rinsed by immersion in the corresponding solvent to remove the chemical residuals from the surface and then dried in nitrogen. Typically, 3 cycles of CdS nanoparticles were pre-assembled on the photoanode through

the SILAR technique and subsequently thin layers of CdSe nanoparticles were grown by chemical bath deposition (CBD).

For CdSe QD-sensitization, a chemical bath solution was prepared by mixing 80 mM $CdSO_4$ and 80 mM sodium selenosulphite (Na_2SeSO_3) solution with 120 mM nitriloacetic acid. The resultant TiO_2 fibrous electrodes were immersed in the chemical bath at 10 °C for 12 hours. Finally, the films were soaked in deionized water and dried with nitrogen. In order to decipher the recombination kinetics at TiO_2–CdS/CdSe–electrolyte interfaces, the passivation layer of ZnS was coated after SILAR sensitization, by alternately dipping it into 0.1 M $Zn(CH_3COO)_2$ and 0.1 M Na_2S solutions for 1 min per dip and subsequently rinsing with Milli-Q ultrapure water. Two SILAR cycles were employed for ZnS coating.

2.3 Device assembly

After fabricating the QD-sensitized electrode by the SILAR process described above, the cell was assembled using a transparent hot-melt 25 μm thick Surilyn ring (DuPont) as a spacer between the QD-sensitized fibrous electrode and the counter-electrode (Pt on FTO glass, chemical deposition of 0.05 M hexachloroplatinic acid in 2-propanol at 450 °C for 30 minutes). The polysulfide electrolyte was introduced through a hole drilled in the counter-electrode that was sealed later. The active area of the cell was 0.16 cm^2 and the samples were irradiated with 1 sun illumination without a mask and using a metallic surface reflector under the cell to backscatter the light that had not been absorbed.

2.4 Characterization techniques

The surface morphology of the samples was probed by using a Hitachi S-4300SE scanning electron microscope (SEM) and a JEOL JEM 2100F field emission transmission electron microscope (TEM). The crystalline structures of pristine and QD-sensitized fibrous electrodes were determined using a thin film X-ray diffractometer (Rigagu Denki Japan) with CuKα radiation. The QDs assembly on the TiO_2 fibrous surface was further testified by X-ray photoelectron spectroscopy (XPS) using a VG Microtech (VG Multilab ESCA 2000 system) X-ray photoelectron spectrometer. The XPS experiment was carried out in a high-vacuum chamber at a base pressure of 3×10^{-9} Torr and the samples were excited with an AlKα X-ray radiation of 1487 eV energy. All the spectra reported in this work are referenced to the C 1s peak (284.6 eV).

The optical absorption spectra of the photoanodes were recorded at 200–800 nm by a Cary 500 UV-vis Varian spectrophotometer. Photovoltaic characteristics of the devices were studied from *J–V* measurements obtained using a FRA-equipped PGSTAT-30 from Autolab and a Keithley 2612 System Source Meter. Measurements were carried out after 10 minutes of light soaking at 1 sun illumination. The cells were illuminated using a solar simulator at AM1.5 G, where the light intensity was adjusted with an NREL-calibrated Si solar cell with a 4a KG-5 filter to 1 sun intensity (100 mW cm^{-2}). The IPCE measurements were performed by employing a 150 W Xe lamp coupled with a computer-controlled monochromator; the photocurrent was measured using an optical power meter 70310 from Oriel Instruments. Impedance spectroscopy (IS) measurements were carried out with a FRA-equipped PGSTAT-30 from Autolab, applying a 20 mV AC signal and scanning in the frequency range between 400 kHz and 0.1 Hz at different forward applied biases. IS was carried out under dark conditions.

3. Results and discussion

3.1 Surface morphology

Scanning electron microscopy (SEM) images of continuous, untreated (UT) TiO_2 nanofibrous membranes on FTO substrates are shown in Fig. 1(a) and surface treated fibers with DMF and THF are presented in Fig. 1(b) and (c) respectively.

Fig. 1(a) clearly indicates that the UT fibers show a smooth surface with 70–100 nm diameter and several micrometers length. After surface pre-treatment with DMF (Fig. 1(b)), the fibrous channels were intertwined and became a rather compact structure. This may be due to the fact that DMF treatment swells the

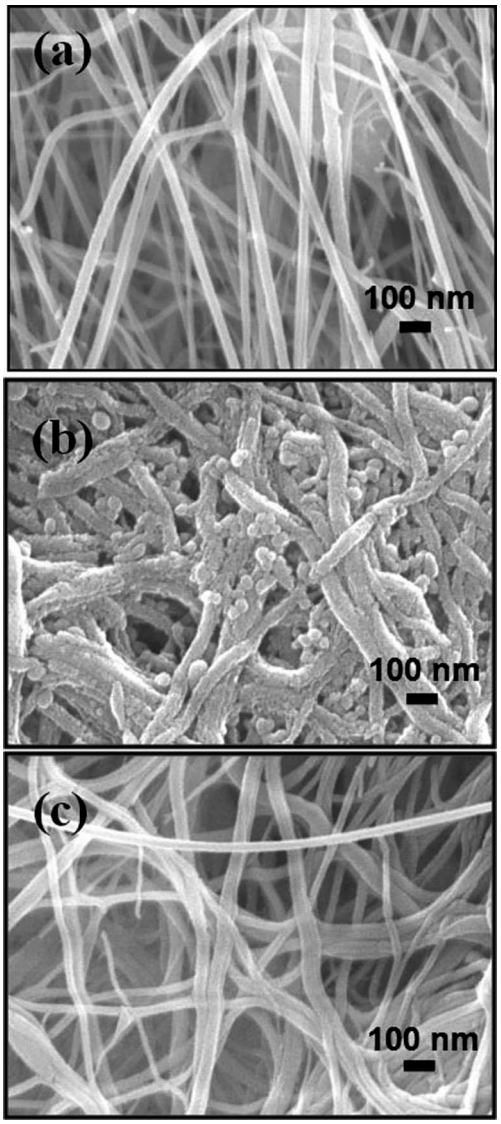

Fig. 1 SEM images of (a) untreated TiO_2, (b) DMF pre-treated TiO_2 and (c) THF vapor pre-treated TiO_2.

PVAc of the fibers, thus resulting in a coagulated fiber structure. This coagulated fiber structure reduces the inter-pore distance between each fiber channel, reducing consequently the effective surface area of the electrode for electrolyte penetration. However, it could improve the electrical contact between the FTO substrate and the fibrous TiO_2 layer. In the case of THF vapor treatment (Fig. 1(c)), the fibrous surface seems etched, which could consequently improve fibers' inter-junction points. Also, the inter-pore distance between fibrous channels is partially retained after the THF pre-treatment. As a consequence, THF treatment produces electrodes to half way between UT and DMF electrodes. Comparing Fig. 1(b) and (c), THF vapor pre-treatment offers fiber reinforcement with lower sacrifice of inter-pore distance than in the case of DMF treatment. In addition, both surface treatments increase the diameter of the fibers compared to the untreated ones.

The pristine and CdS QDs pre-assembled TiO_2 fibrous surface is presented in Fig. 2. Fig. 2(a) provides a view of the fibrous surface texture in close proximity, where the TiO_2 grains are highly distinguished and well crystallized. The estimated lattice fringe of about ~0.35 nm confirms the existence of the (101) anatase TiO_2 phase in the fibers, see Fig. 2(c). Fig. 2(c) shows the CdS QDs pre-assembled on a TiO_2 fiber surface by increasing the magnification scale to 5 nm; it seems that CdS QDs are randomly covered on the fibrous surface. The lattice fringe of about ~0.32 nm derived from Fig. 2(d) endorses the (101) hexagonal greenockite structure of CdS. The co-sensitization of CdSe on TiO_2–CdS QDs is confirmed by Fig. 3. The closer view at the 5 nm scale clearly shows that CdSe QDs densely wrap the TiO_2–CdS QDs surface. The lattice fringes were analyzed randomly on different positions of the fibrous surface and found to be 0.34 nm, Fig. 3(b), which correspond to the cubic CdSe structures. The elemental mapping of Ti, O, Cd, S and Se was recorded and is presented in Fig. 3(c), observing a uniform distribution of sensitizing elements along the fiber length. The estimated crystallite structures of pristine and CdS/CdSe QD-sensitized TiO_2 electrodes were tested using XRD (Fig. S1†) and they are in good correlation with TEM observations. The chemical environment of the CdS/CdSe sensitized TiO_2 fibrous surface is further testified by X-ray photoelectron spectroscopy (XPS) (Fig. S2†).

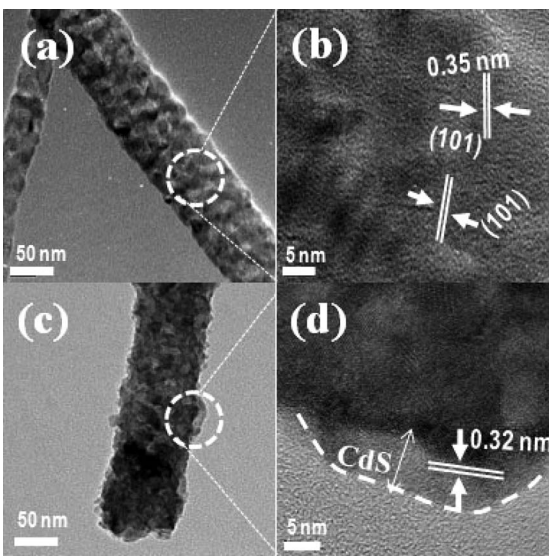

Fig. 2 TEM images of (a) untreated TiO_2, (b) highly magnified images of the circled area of the TiO_2 fiber in (a) at the 5 nm scale: crystalline lattice of anatase TiO_2 and (c) TEM images of self-assembled CdS QDs on a fibrous surface, (d) highly magnified images of the circled area in (c) at the 5 nm scale: note that CdS QDs randomly coated on the TiO_2 fibrous surface are indicated.

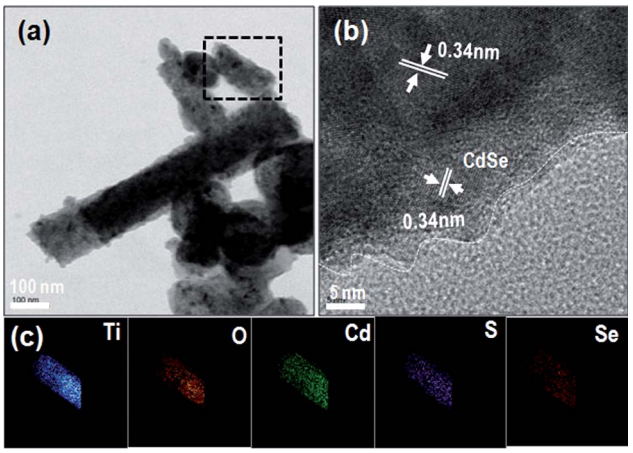

Fig. 3 HRTEM images of CdSe QDs coated onto a CdS pre-assembled TiO_2 fibrous membrane. (b) Highly magnified images of the circled area in Fig. 2(c) at the 5 nm scale, (c) elemental map of the square box in (a), displaying Zn, O, Cd, Se and S spatial elemental distribution.

3.2 Photovoltaic characteristics

In order to decipher the influence of chemical pre-treatment and post-layer treatment on QD-sensitized TiO_2 fibrous solar cells, devices prepared with different treatments have been analyzed. In the first step, we studied QDSCs performance of QD-sensitized electrodes prepared with untreated fiber electrodes (UT) and electrodes treated with DMF and THF treatments. The current–voltage (J–V) measurements of these cells are presented in Fig. 4(a) and their corresponding photovoltaic parameters are listed in Table 1. IPCE measurements can be found in Fig. 4(b). Note that the short circuit photocurrent predicted by these IPCE measurements is lower than those provided in Fig. 4(a) and in Table 1 due to two facts: J–V measurements have been carried out without a mask and using a back light reflector. From Table 1, the THF-treated electrodes show higher photoconversion efficiency (2.1%) than that of UT and DMF treated electrodes. The improvement of the device performance can be mainly attributed to the enhancement in V_{oc} and J_{sc}.

Fig. 5(a) and (b) show respectively the light absorption and reflectance of UT, DMF and THF electrodes. As expected, there is a good correlation between the obtained absorption and the IPCE pattern. In view of sensitizer loading, DMF and THF-treated electrodes show less QDs accommodation than UT electrodes, the DMF-sensitized electrode being the sample with the lowest absorbance. However, THF-QDSCs result in a photocurrent similar to UT-QDSCs, in fact slightly higher, while the DMF cell presents a lower photocurrent. On the other

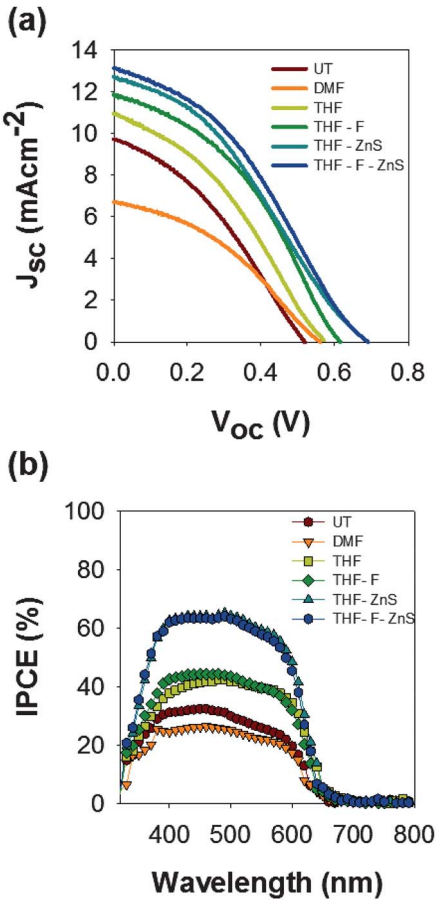

Fig. 4 (a) *J–V* curves and (b) IPCE spectra of QDSCs using different surface treated TiO_2 nanofibrous electrodes: UT, DMF, THF, THF + F, THF + ZnS and THF + F + ZnS electrodes with CdS/CdSe QDs.

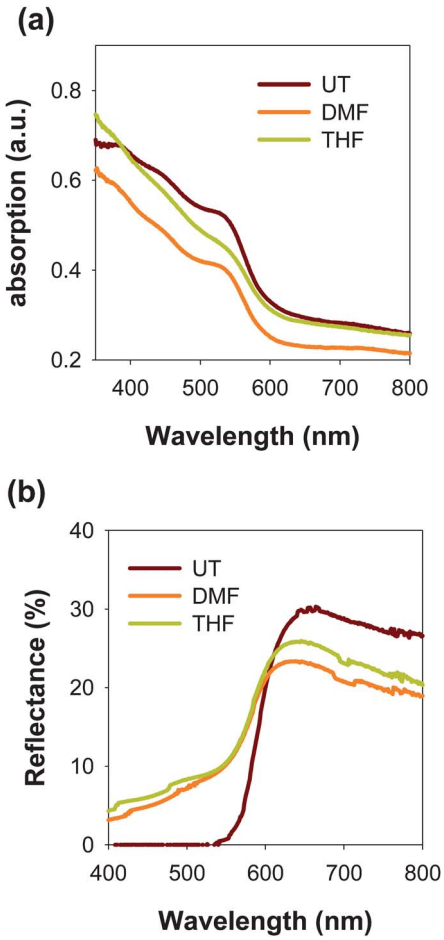

Fig. 5 (a) Optical absorption spectra of CdSe/CdS QDs in different TiO_2 fibrous electrodes and (b) reflection spectra of CdSe/CdS QD-sensitized TiO_2 fibrous electrodes.

Table 1 Photovoltaic parameters of semiconductor-sensitized solar cells using pristine and surface-modified TiO_2 fibrous photoanodes with 2.4 μm thickness (without a mask, active area: 0.16 cm^2). The β parameter following the β-recombination model is also included. β takes into account the non-linear recombination observed for sensitized solar cells.[50,51] UT: untreated fiber; DMF: dimethylformamide treated; THF: tetrahydrofuran vapor treated; THF–F: THF vapor treated and a post F-ion treatment; THF–ZnS: THF-vapor-treated fiber and a ZnS passivation layer on CdS/CdSe QDs; and THF–F–ZnS: THF-vapor-treated fiber plus post F ion treatment and also a final ZnS passivation layer on CdS/CdSe QDs

Samples	V_{oc} (V)	J_{sc} (mA cm^{-2})	FF [%]	η [%]	β
UT	0.52	9.53	36.0	1.8	0.32
DMF	0.56	6.52	36.0	1.4	0.39
THF	0.57	9.74	39.0	2.1	0.43
THF–F	0.61	11.4	40.2	2.8	
THF–ZnS	0.69	12.8	34.1	3.0	0.35
THF–F–ZnS	0.69	13.0	35.9	3.2	0.34

hand, treated QDSCs present in both cases higher V_{oc} than the UT sample (see Table 1).

3.2.1 Post-layer process. The higher performance observed for THF cells led us to choose these samples as reference for the study of post-layer processes in order to obtain a further improvement of the cell performance. We investigated fluorine (F^-) ion treatment on THF treated fibers (after sintering) similar to our previous report.[47] The THF electrodes were soaked in the as-prepared 1 M NH_4F solution by dissolving the NH_4F powder in Milli-Q water for 5 minutes. After the fluorine treatment, the samples were rinsed with Milli-Q water for 1 minute and dried with a nitrogen flow. The QDSC is assembled with an F ion-treated electrode, hereafter represented as 'THF–F'. Along with this electrode, another post-layer coating of ZnS layer was applied by the SILAR process as explained in the Experimental section. The QDSCs assembled with ZnS passivation coating (after QDs loading) are called THF–ZnS, while the cell prepared with a combination of F^- ion treatment (before QD deposition) and ZnS coating is referred to hereafter as THF–F–ZnS. The *J–V* performances of post-layer coated QDSCs are compared in Fig. 4, and Table 1 provides the solar cell parameters of these cells.

Under F^- ion treatment, THF–F cells showed 33% improvement (η = 2.8%) through increasing photocurrent generation (11.4 mA cm^{-2}) and improving the V_{oc} (0.61 V) of the device. The beneficial effect of F^- ion treatment on device performance can be explained by retarding the charge recombination through TiO_2 surface states by managing oxygen vacancies *via* formation of the Ti–F bond by surface fluorination reaction (Ti–OH + $F^- \rightarrow$ Ti–F + OH^-).[47] Fluorine treatment produces a decrease of

the recombination rate in CdS and CdSe QDSCs,[47] resulting in an enhancement of V_{oc}, with a concomitant improvement of J_{sc}, as can be observed in Fig. 4.

Concerning ZnS post-layer coating on CdS/CdSe QDs, the THF device performance is markedly enhanced by increasing the V_{oc} from 0.57 V to a significantly high value of 0.69 V. This clearly indicates that the ZnS post-layer on the QD–TiO_2 fibrous surface plays a vital role in QDSCs performance, in the same way that it has been observed in other electrode configurations.[48–50] The combined configuration of F and ZnS coating (THF–F–ZnS) results in a slightly superior device performance, $\eta = 3.2\%$, with also a remarkable $V_{oc} = 0.69$ V and $J_{sc} = 13.0$ mA cm^{-2}. The overall comparison of QDSCs, Table 1, suggests that the THF device results in high performance upon inclusion of post-layer coatings. However, the analyzed cells in this work still have inferior overall performance, with a low fill factor of 35–40%, compared to highly efficient QDSCs (FF = 60%) due to the bad charge transfer between the platinized counter-electrode and the polysulfide electrolyte.[11,51,52,57] The poisoning effect of polysulfide on Pt increases the charge transfer resistance at the counter-electrode. This charge transfer resistance acts as a series resistance that affects the FF deleteriously. It is anticipated that replacing the Pt counter-electrode with robust carbon,[28,53,54] metal sulfides[55–57] or metal sulfide–carbon composites[58] will further improve the cell efficiency. However, the use of a platinized counter-electrode allows an efficient cell sealing, increasing cell stability and the accuracy of long time measurements, such as impedance measurements. In fact the reported results (Fig. 4 and Table 1) were performed one day after cell preparation.

Further characterization of QDSCs has been performed by impedance spectroscopy (IS) measurements. The obtained chemical capacitance, C_μ (Fig. 6(a)), and recombination resistance, R_{rec} (Fig. 6(b)), are plotted against the voltage drop in the sensitized electrode, V_F, removing the effect of the series resistance.[59] A clear change in the slope obtained for C_μ is observed after DMF or THF treatments, evolving in a similar way for both treatments (see Fig. 6(a)). The slope and the absolute capacitance do not vary with the post-layer treatments with ZnS and F plus ZnS. C_μ reflects the density of states (DOS) of TiO_2.[59] DMF and THF treatments produce a change in the DOS distribution of TiO_2 fibrous electrodes. Further treatments, F or ZnS, do not produce any additional change in DOS distribution. Thus the surface nature of TiO_2 fibrous electrodes is radically modified after DMF and THF treatments. In addition, these treatments also produce a dramatic decrease of the recombination rate and consequently an increase of R_{rec} (see Fig. 6(b)). The reduction of the recombination rate results in the treated samples, both DMF and THF, having higher V_{oc} than UT cells. The lower QD loading in DMF cells indicates that the final performance of this cell is lower than the performance of the UT sample, due to a lower J_{sc}. On the other hand, in the case of THF cells, the lower recombination rate with only a moderate decrease of QD loading in comparison with UT samples produce a final performance higher than that of the UT sample. Thus DMF and THF treatments reduce significantly the recombination of TiO_2 fibrous electrodes, but at the cost of a lower QD loading. In the case of THF treatment where the QD loading reduction is not very high, the reduction of recombination finally produces more efficient electrodes.

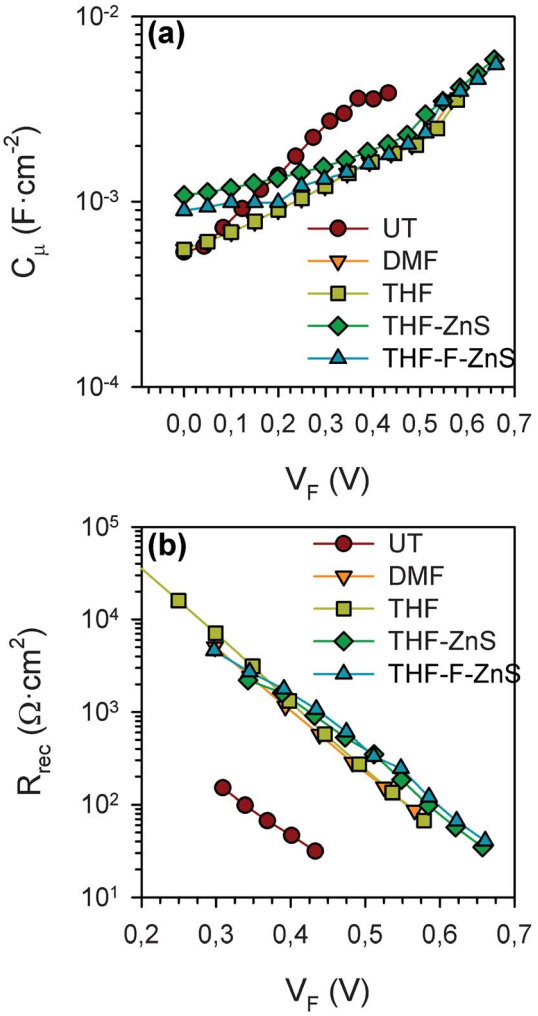

Fig. 6 (a) Chemical capacitance and (b) recombination resistance of pre-treated and post-layer coated QDSCs.

Concerning the effect of post-layer treatments (ZnS and F–ZnS), there is only a slight increase in the recombination resistance, so the cell performance improvement detected in these cells cannot be mainly attributed to a reduction in the recombination rate. The main effect of ZnS coating is the passivation of the CdSe QDs, as has been discussed by Guijarro *et al.*[48] QD passivation produces a significant enhancement of photocurrent as the rate of internal recombination (before injection into TiO_2) of photoexcited electrons in the QD decreases and consequently the number of electrons injected into TiO_2 increases. It is important to note that there is an evolution of the slope of log(R_{rec}) *vs.* V_F. From this slope the β parameter can be extracted. β is the exponent of the non-linear recombination observed empirically in sensitized solar cells, and it is closely related to the recombination process.[59,60] The obtained β values are depicted in Table 1. The UT cell presents a value of 0.32 that increases with DMF and THF treatments. After ZnS coating, the β value decreases again, as has been previously observed.[61] It has been suggested that the β value relates to the charge transfer *via* an exponential distribution of surface states, with parameter T_0, which gives $\beta = 0.5 + T/T_0$.[59,60] But, further research is needed to relate the β value to the exact microscopic recombination process.

Based on the above arguments, we have summarized the recombination behavior of the analyzed samples schematically in Scheme 1. In Scheme 1, recombination pathways are denoted by the recombination rates r_1, and r_2. r_1 takes into account the recombination of the electrons in TiO_2 with acceptor states in the QDs and/or the electrolyte. These electrons have been previously photogenerated in the QDs and injected into TiO_2. On the other hand r_2 encompasses the recombination of the photogenerated electrons *before* being injected into TiO_2. r_2 includes several contributions such as the recombination of the photogenerated electron with acceptor species in the electrolyte and the internal recombination in the QD of the electron–hole pair before they can be injected into another media. Internal recombination processes can follow radiative and non-radiative recombination that can be mediated by QD surface states. The UT sample presents high r_1, Scheme 1(a); further research is being currently performed in order to determine what is the main cause of the high recombination rate: poor electrical contact between FTO and fibers surface or the particular DOS of untreated nanofibers. THF vapor treatment reduces r_1, Scheme 1(b), as it has been demonstrated by IS. Fluorine treatment produces an additional reduction of r_1, Scheme 1(c).[52] Finally ZnS coating acts mainly by reducing r_2, Scheme 1(d).[53,54]

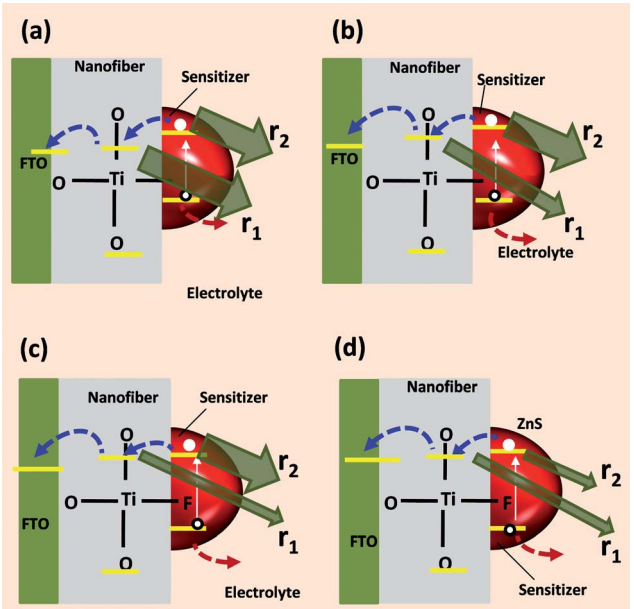

Scheme 1 Charge transport and charge recombination at different configurations. (a) QD-sensitized untreated fiber; (b) QD-sensitized THF treated fiber; (c) QD-sensitized F-ion post-treated fiber surface and (d) QD-sensitized F-ion post-treated fiber surface with a ZnS surface passivation layer. White arrows indicate photogeneration of the electron–hole pair in the sensitizer. Blue dashed arrows indicate the electron injection first into TiO_2 and later into FTO, while red dashed arrows indicate the hole injection into the polysulfide electrolyte. Green transparent arrows indicate the two recombination pathways: recombination of electrons in the TiO_2 (characterized by recombination rate r_1), and recombination of electrons in the QD, before electron injection into TiO_2 (characterized by recombination rate r_2). The thickness of the arrows is proportional to the recombination rate.

4. Conclusion

Highly dense, continuous and nanostructured TiO_2 fibrous membranes have been directly prepared on a transparent conducting substrate and showed feasible photo-anode performance with the aid of visible light harvesting semiconductors, CdS and CdSe QDs. We demonstrated a systemic interfacial engineering protocol on QD-sensitized TiO_2 fibrous membrane electrodes for promoting their photo-conversion efficiency. We found that THF vapor treatment on as-deposited TiO_2 fibrous membranes markedly improved the physical adhesion of fibers with the FTO substrate and also enhanced the open-circuit potential from $V_{oc} = 0.52$ V to $V_{oc} = 0.57$ V due to a reduction in the recombination rate. F-ion post-treatment on the TiO_2 fibrous membrane improves both V_{oc} (0.61 V) and J_{sc} (11.4 mA cm^{-2}) of the device with an overall efficiency of 2.8%. Concurrently, further V_{oc} enhancement is observed after ZnS coating on a sensitizer layer (QDs), which strikingly improves the V_{oc} (0.69 V) by passivating the QDs. With the combined THF–F ion treatment with the ZnS passivation layer on the QD-sensitizer, our proposed TiO_2 fibrous photoanode yielded a device performance of 3.2% with a remarkable $V_{oc} = 0.69$ V compared with most of the reports existing in the literature. This interfacial engineering approach on fibrous membranes is directly relevant to the design of photoanodes for wide energy conversion assemblies including water splitting solar hydrogen generation, hybrid (QDs–dye) excitonic solar cells, and light driven photocatalysts, in which electrolyte penetration, faster electron transport, and high internal surface area are key to achieving high efficiency.

Acknowledgements

This work was supported by the Engineering Research Center Program through a National Research Foundation of Korea (NRF) grant funded by the Ministry of Education, Science and Technology (MEST) (no. 2012-0000591) and also by the World Class University (WCU) program (no. R31-2008-000-10092), the Ministerio de Educación y Ciencia of Spain under the project HOPE CSD2007-00007 (Consolider-Ingenio 2010) JES-NANOSOLAR PLE2009-0042, MAT 2010-19827 and by Generalitat Valenciana under project PROMETEO/2009/058.

Notes and references

1 M. Gratzel, *Nature*, 2001, **414**, 338–344.
2 S. Ruhle, M. Shalom and A. Zaban, *ChemPhysChem*, 2010, **11**, 2290–2304.
3 P. V. Kamat, *J. Phys. Chem. C*, 2008, **112**, 18737–18753.
4 I. Mora-Sero and J. Bisquert, *J. Phys. Chem. Lett.*, 2010, **1**, 3046–3052.
5 A. M. Smith and S. M. Nie, *Acc. Chem. Res.*, 2010, **43**, 190–200.
6 W. A. Tisdale, K. J. Williams, B. A. Timp, D. J. Norris, E. S. Aydil and X. Y. Zhu, *Science*, 2010, **328**, 1543–1547.
7 V. I. Klimov, *J. Phys. Chem. B*, 2006, **110**, 16827–16845.
8 J. B. Sambur, T. Novet and B. A. Parkinson, *Science*, 2010, **330**, 63–66.
9 O. E. Semonin, J. M. Luther, S. Choi, H. Y. Chen, J. B. Gao, A. J. Nozik and M. C. Beard, *Science*, 2011, **334**, 1530–1533.
10 P. Sudhagar, J. H. Jung, S. Park, R. Sathyamoorthy, H. Ahn and Y. S. Kang, *Electrochim. Acta*, 2009, **55**, 113–117.
11 I. Mora-Sero, S. Gimenez, T. Moehl, F. Fabregat-Santiago, T. Lana-Villareal, R. Gomez and J. Bisquert, *Nanotechnology*, 2008, **19**, 424007.

12 M. Samadpour, A. I. Zad, N. Taghavinia and M. Molaei, *J. Phys. D: Appl. Phys.*, 2011, **44**, 045103.
13 Y. L. Lee and Y. S. Lo, *Adv. Funct. Mater.*, 2009, **19**, 604–609.
14 S. J. Moon, Y. Itzhaik, J. H. Yum, S. M. Zakeeruddin, G. Hodes and M. Gratzel, *J. Phys. Chem. Lett.*, 2010, **1**, 1524–1527.
15 C. Chen, Y. Xie, G. Ali, S. H. Yoo and S. O. Cho, *Nanoscale Res. Lett.*, 2011, **6**, 462.
16 A. Braga, S. Gimenez, I. Concina, A. Vomiero and I. Mora-Sero, *J. Phys. Chem. Lett.*, 2011, **2**, 454–460.
17 H. J. Lee, P. Chen, S. J. Moon, F. Sauvage, K. Sivula, T. Bessho, D. R. Gamelin, P. Comte, S. M. Zakeeruddin, S. Il Seok, M. Gratzel and M. K. Nazeeruddin, *Langmuir*, 2009, **25**, 7602–7608.
18 P. Sudhagar, J. H. Jung, S. Park, Y. G. Lee, R. Sathyamoorthy, Y. S. Kang and H. Ahn, *Electrochem. Commun.*, 2009, **11**, 2220–2224.
19 V. Gonzalez-Pedro, X. Q. Xu, I. Mora-Sero and J. Bisquert, *ACS Nano*, 2010, **4**, 5783–5790.
20 S. Buhbut, S. Itzhakov, E. Tauber, M. Shalom, I. Hod, T. Geiger, Y. Garini, D. Oron and A. Zaban, *ACS Nano*, 2010, **4**, 1293–1298.
21 H. Choi, R. Nicolaescu, S. Paek, J. Ko and P. V. Kamat, *ACS Nano*, 2011, **5**, 9238–9245.
22 M. Shalom, J. Albero, Z. Tachan, E. Martinez-Ferrero, A. Zaban and E. Palomares, *J. Phys. Chem. Lett.*, 2010, **1**, 1134–1138.
23 I. Mora-Seró, D. Gross, T. Mittereder, A. A. Lutich, A. Susha, T. Dittrich, A. Belaidi, R. Caballero, F. Langa, J. Bisquert and A. L. Rogach, *Small*, 2010, **6**, 221–225.
24 J. H. Im, C. R. Lee, J. W. Lee, S. W. Park and N. G. Park, *Nanoscale*, 2011, **3**, 4088–4093.
25 Q. Zhang, X. Guo, X. Huang, S. Huang, D. Li, Y. Luo, Q. Shen, T. Toyoda and Q. Meng, *Phys. Chem. Chem. Phys.*, 2011, **13**, 4659–4667.
26 A. Yella, H. W. Lee, H. N. Tsao, C. Y. Yi and A. K. Chandiran, *Science*, 2011, **334**, 1203.
27 P. Sudhagar, T. Song, D. H. Lee, I. Mora-Sero, J. Bisquert, M. Laudenslager, W. M. Sigmund, W. I. Park, U. Paik and Y. S. Kang, *J. Phys. Chem. Lett.*, 2011, **2**, 1984–1990.
28 P. Sudhagar, E. Ramasamy, W. H. Cho, J. Lee and Y. S. Kang, *Electrochem. Commun.*, 2011, **13**, 34–37.
29 F. Hetsch, X. Q. Xu, H. K. Wang, S. V. Kershaw and A. L. Rogach, *J. Phys. Chem. Lett.*, 2011, **2**, 1879–1887.
30 V. Jovanovski, V. Gonzalez-Pedro, S. Gimenez, E. Azaceta, G. Cabanero, H. Grande, R. Tena-Zaera, I. Mora-Sero and J. Bisquert, *J. Am. Chem. Soc.*, 2011, **133**, 20156–20159.
31 G. Hodes, *J. Phys. Chem. C*, 2008, **112**, 17778–17787.
32 P. P. Boix, G. Larramona, A. Jacob, B. Delatouche, I. Mora-Seró and J. Bisquert, *J. Phys. Chem. C*, 2012, **116**, 1579–1587.
33 M. Samadpour, S. Gimenez, A. Iraji Zad, N. Taghavinia and I. Mora-Sero, *Phys. Chem. Chem. Phys.*, 2012, **14**, 522–528.
34 E. Ghadiri, N. Taghavinia, S. M. Zakeeruddin, M. Gratzel and J. E. Moser, *Nano Lett.*, 2010, **10**, 1632–1638.
35 S. Huang, X. Guo, X. Huang, Q. Zhang, H. Sun, D. Li, Y. Luo and Q. Meng, *Nanotechnology*, 2011, **22**, 315402.
36 N. Tetreault, E. Horvath, T. Moehl, J. Brillet, R. Smajda, S. Bungener, N. Cai, P. Wang, S. M. Zakeeruddin, L. Forro, A. Magrez and M. Gratzel, *ACS Nano*, 2010, **4**, 7644–7650.
37 T. S. Kang, A. P. Smith, B. E. Taylor and M. F. Durstock, *Nano Lett.*, 2009, **9**, 601–606.
38 J. H. Park, T. W. Lee and M. G. Kang, *Chem. Commun.*, 2008, 2867–2869.
39 G. K. Mor, K. Shankar, M. Paulose, O. K. Varghese and C. A. Grimes, *Nano Lett.*, 2006, **6**, 215–218.
40 S. Huang, Q. Zhang, X. Huang, X. Guo, M. Deng, D. Li, Y. Luo, Q. Shen, T. Toyoda and Q. Meng, *Nanotechnology*, 2010, **21**, 375201.
41 E. Ghadiri, N. Taghavinia, S. M. Zakeeruddin, M. Gratzel and J. E. Moser, *Nano Lett.*, 2010, **10**, 1632–1638.
42 P. S. Archana, R. Jose, C. Vijila and S. Ramakrishna, *J. Phys. Chem. C*, 2009, **113**, 21538–21542.
43 P. Joshi, L. F. Zhang, D. Davoux, Z. T. Zhu, D. Galipeau, H. Fong and Q. Q. Qiao, *Energy Environ. Sci.*, 2010, **3**, 1507–1510.
44 M. Y. Song, D. K. Kim, K. J. Ihn, S. M. Jo and D. Y. Kim, *Nanotechnology*, 2004, **15**, 1861–1865.
45 M. Y. Song, D. K. Kim, K. J. Ihn, S. M. Jo and D. Y. Kim, *Synth. Met.*, 2005, **153**, 77–80.
46 K. Onozuka, B. Ding, Y. Tsuge, T. Naka, M. Yamazaki, S. Sugi, S. Ohno, M. Yoshikawa and S. Shiratori, *Nanotechnology*, 2006, **17**, 1026–1031.
47 M. Samadpour, P. P. Boix, S. Gimenez, A. I. Zad, N. Taghavinia, I. Mora-Sero and J. Bisquert, *J. Phys. Chem. C*, 2011, **115**, 14400–14407.
48 N. Guijarro, J. M. Campina, Q. Shen, T. Toyoda, T. Lana-Villarreal and R. Gomez, *Phys. Chem. Chem. Phys.*, 2011, **13**, 12024–12032.
49 I. Mora-Seró, S. Giménez, F. Fabregat-Santiago, R. Gómez, Q. Shen, T. Toyoda and J. Bisquert, *Acc. Chem. Res.*, 2009, **42**, 1848–1857.
50 Q. Shen, J. Kobayashi, L. J. Diguna and T. Toyoda, *J. Appl. Phys.*, 2008, **103**, 084304.
51 S. Gimenez, I. Mora-Sero, L. Macor, N. Guijarro, T. Lana-Villarreal, R. Gomez, L. J. Diguna, Q. Shen, T. Toyoda and J. Bisquert, *Nanotechnology*, 2009, **20**, 295204.
52 G. Hodes, J. Manassen and D. Cahen, *J. Electrochem. Soc.*, 1980, **127**, 544–549.
53 B. Fang, M. Kim, S. Q. Fan, J. H. Kim, D. P. Wilkinson, J. Ko and J. S. Yu, *J. Mater. Chem.*, 2011, **21**, 8742–8748.
54 S. Q. Fan, B. Fang, J. H. Kim, J. J. Kim, J. S. Yu and J. Ko, *Appl. Phys. Lett.*, 2010, **96**, 063501.
55 M. H. Deng, S. Q. Huang, Q. X. Zhang, D. M. Li, Y. H. Luo, Q. Shen, T. Toyoda and Q. B. Meng, *Chem. Lett.*, 2010, **39**, 1168–1170.
56 Z. S. Yang, C. Y. Chen, C. W. Liu and H. T. Chang, *Chem. Commun.*, 2010, **46**, 5485–5487.
57 Z. Tachan, M. Shalom, I. Hod, S. Ruhle, S. Tirosh and A. Zaban, *J. Phys. Chem. C*, 2011, **115**, 6162–6166.
58 J. G. Radich, R. Dwyer and P. V. Kamat, *J. Phys. Chem. Lett.*, 2011, **2**, 2453–2460.
59 F. Fabregat-Santiago, G. Garcia-Belmonte, I. Mora-Sero and J. Bisquert, *Phys. Chem. Chem. Phys.*, 2011, **13**, 9083–9118.
60 J. Bisquert and I. Mora-Seró, *J. Phys. Chem. Lett.*, 2010, **1**, 450–456.
61 I. Hod, V. González-Pedro, Z. Tachan, F. Fabregat-Santiago, I. Mora-Seró, J. Bisquert and A. Zaban, *J. Phys. Chem. Lett.*, 2011, **2**, 3032–3035.